1 # A study on the longitudinal compression strength of fibre reinforced

2 # composites under uniaxial and off-axis loads using cross-ply laminate

3 # specimens

4 Daniel Thomson[a], Hao Cui[b,*], Borja Erice[a,c], Nik Petrinic[a]

5 [a]Department of Engineering Science, University of Oxford, Oxford, United Kingdom

6 [b]School of Aerospace, Transport and Manufacturing, Cranfield, United Kingdom

7 [c]Structural Impact Laboratory (SIMLab), Department of Structural Engineering,

8 Norwegian University of Science and Technology (NTNU),

9 Richard Birkelands vei 1A, NO-7491 Trondheim, Norway

10 **Abstract**

11 Longitudinal compression testing of unidirectional FRP laminates remains a challenge due to the

12 difficulty in applying high compressive loads without stress concentrations and boundary effects

13 leading to premature failure. This work aims to critically evaluate different specimen designs and

14 laminate configurations, cross-ply in particular, for the determination of longitudinal compression

15 properties of unidirectional plies.

16 To this end, a comprehensive experimental campaign has been carried out, comparing strength,

17 stiffness, and failure modes across different specimen designs and laminate configurations. The

18 investigated cross-ply specimens produced comparable results without many of the issues observed

19 in the testing unidirectional material and, therefore, are strongly recommended for the determination

20 of longitudinal compressive strength.

21 Finally, the cross-ply material was tested under off-axis compression to study the effects of shear on

22 the longitudinal compression strength using a series of compression specimens cut at different angles

23 between 0 and 15° to the direction of the laminate.

24 *Keywords:* Polymer matrix composites; Mechanical properties; Longitudinal compression; Buckling.

*Corresponding author, hao.cui@cranfield.ac.uk

1 Introduction

The compressive strength in fibre direction is of great interest to the design and analysis of laminated composite structures. The longitudinal compressive failure (so called fibre kinking failure) is triggered by inter-fibre damage, which results in local buckling of fibres causing catastrophic material failure. Much work has been done over the years to try to understand the underlying physical phenomena behind this type of failure and its main contributing factors so that it can be more accurately predicted and designed against [1–5]. However, without accurate or reliable experimental measurements, these theories cannot be properly evaluated. The accurate characterization of the critical load in this failure mode remains problematic because the strength in the fibre direction is much higher than that in the transverse direction, which, if the tests are not designed and carried out correctly, often causes matrix failure to occur before the fibre micro-buckling can occur [6,7].

Premature matrix splitting of this kind can be caused by the transverse stresses through the thickness of the laminate that arise due to the Poisson effect and stress concentrations at specimen boundaries. Commonly, the solution to mitigate the effect of boundary conditions has been to add clamping fixtures that strengthen the matrix at the loading ends of the specimen and help to distribute the applied load by transmitting some of the compression through shear in the clamped interfaces [6,8]. However, this introduces the risk of new stress concentrations at the fixture boundaries and of over constraining the specimen, making the results highly sensitive to the test operator and set-up conditions, as reported in [6].

Another proposed solution has been the use of specimens with waisted cross-section area that prevent fracture from occurring close to the specimen boundaries. However, the change in cross-section along with the relative low strength of the matrix can also cause critical stress concentrations that may eventually lead to premature splitting.

49 In short, the determination of longitudinal compression strength properties using unidirectional (UD)

50 material can be quite problematic and the high sensitivity to boundary conditions should be a cause

51 for concern any time experiments of this kind are being considered. The large variation in reported

52 compressive strength measurements in [6,7,9] for the UD HexPly® IM7-8552 material system serve

53 as a good example.

54 Because of these issues, the extraction of longitudinal ply properties from multidirectional (MD) or

55 cross-ply (CP) laminates, using classical lamination theory (CLT) has been suggested as a more

56 viable alternative [6,10,11]. However, previous experimental studies have always shown significant

57 differences between the strength measurements obtained from UD and MD laminates. For the IM7-

58 8552 material, for example, Lee and Soutis [6] and Ploeckl et al. [7] reported strength measurements

59 from quasi-isotropic (QI) around 20% higher than the UD material. The use of CP laminates was

60 also explored in the 1990s [10] and higher strengths than the plain UD material were again observed.

61 Based on this previous work, it remains unclear whether the behaviour of MD laminate

62 configurations under longitudinal compression can be representative of UD material and vice versa.

63 However, if this can be established, the use of MD configurations, which have been shown to solve

64 many of the issues that have plagued longitudinal compression in UD specimens, may alleviate the

65 need for complex fixtures and specimen designs and, in turn, simplify the testing process and

66 increase the level of confidence in the results.

67 Therefore, in this study, a systematic experimental campaign has been carried out to: (i) determine

68 the most suitable test and specimen configurations for the measurement of longitudinal compression

69 strength; (ii) evaluate the equivalence between longitudinal compression properties obtained from

70 UD and CP material, in particular; and (iii) investigate the applicability of CP material for the

71 determination of UD failure envelope in combined loading cases (longitudinal compression and in-

72 plane shear), which can be used to evaluate 3D fibre kinking failure theories and criteria.

2 Methodology and experimental set-up

2.1 Specimen configuration

The specimens for all experiments were cut from two different HexPly® IM7-8552 [12] composite plates with different ply lay-ups, UD ($[0°]_{26}$) and CP ($[0°/90°]_{4S}$). Both laminates were manufactured together in the same facility to ensure similar quality levels between the two, while noting that local fibre architecture will naturally differ slightly between UD and MD laminates. In addition, all specimens were carefully ground and polished to ensure their two loading faces were parallel with adequate surface quality to a tolerance of ±0.05 mm. This was done, in conjunction with the test set-up described in section 2.2, to minimise the possibility of bending in the specimens due to imperfections in the specimen, fixture or test procedure, which could otherwise affect the quality of the results [8].

The aim for the first set of experiments was to get an accurate measure of the longitudinal compressive strength of the unidirectional material as well as investigating different specimen designs and the effects of different boundary conditions. The different specimen configurations tested, shown in Figure 1, were (a) a simple unclamped cuboidal (rectangular) specimen (UD Cub), (b) an unclamped waisted, or dog-bone, design (UD DBU), (c) a waisted dog-bone specimen with clamping fixtures (UD DBC), and (d) a clamped dog-bone specimen with adhesively bonded GFRP end tabs (UD tabbed DBC) to relax the constraint of the clamping fixtures on the UD material. A gauge section of 5mm x 5mm was kept constant throughout all specimen designs, with a nominal thickness of 2mm.
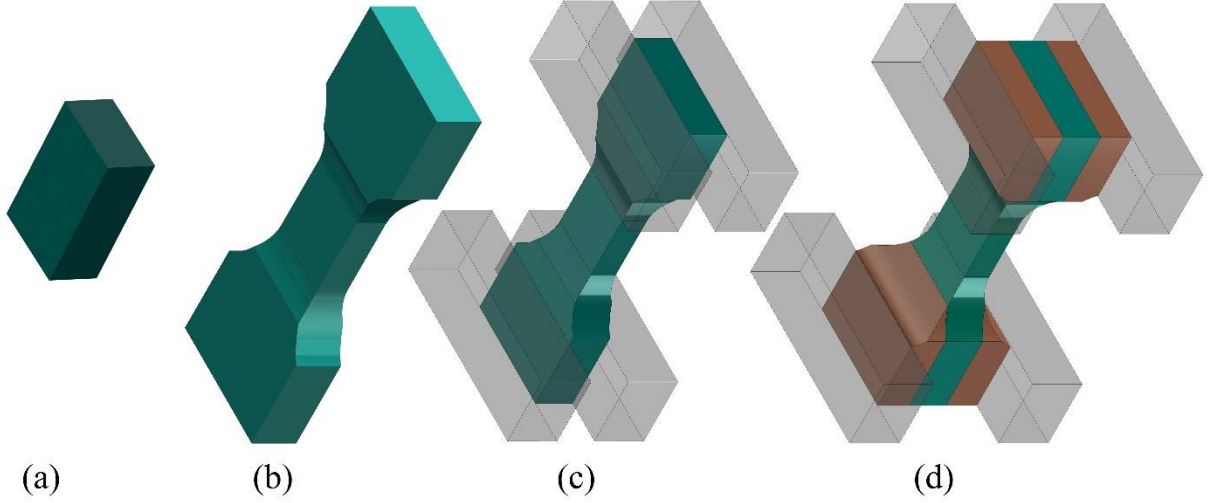
93

Figure 1. *Unidirectional laminate specimen designs: (a) cuboid (UD Cub), (b) unclamped dog-bone*

(UD DBU), (c) clamped dog-bone (UD DBC), and (d) clamped dog-bone with GFRP end tabs (UD

Tabbed DBC).

Next, two different cross-ply specimens were tested to compare against the previous UD results and

study whether the effects of the boundary conditions were also as critical on the multi-directional

laminate. The specimen configurations, shown in Figure 2, were (a) a simple unclamped cuboid (CP

Cub) similar to the UD Cub design in Figure 1 (a), and (b) a clamped dog-bone specimen (CP DBC)

similar to the UD DBC design in Figure 1 (c). Longitudinal material, or ply properties were extracted

from the overall axial response using classical lamination theory (CLT) as described in [11].

First the **ABD** matrix, $\begin{Bmatrix} N \\ M \end{Bmatrix} = \begin{bmatrix} A & B \\ B & D \end{bmatrix} \begin{Bmatrix} \varepsilon^0 \\ K \end{Bmatrix}$, which relates the deformation of the laminate given by

the in-plane strains $\boldsymbol{\varepsilon}^0 = \{\varepsilon_{11}^0 \ \varepsilon_{22}^0 \ \varepsilon_{12}^0 \}^T$ and the laminate curvatures $\boldsymbol{K} = \{\kappa_{11} \ \kappa_{22} \ \kappa_{12} \}^T$ to the

resultant in-plane axial forces $\boldsymbol{N} = \{N_{11} \ N_{22} \ N_{12} \}^T$ and moments $\boldsymbol{M} = \{M_{11} \ M_{22} \ M_{12} \}^T$ per unit

width is computed as:

$$A_{ij} = \sum_{k=1}^n \bar{Q}_{ij}^k (z_k - z_{k-1}) \tag{1}$$

$$B_{ij} = \frac{1}{2} \sum_{k=1}^n \bar{Q}_{ij}^k (z_k^2 - z_{k-1}^2) \tag{2}$$

109 $$D_{ij} = \frac{1}{3}\sum_{k=1}^{n} \bar{Q}_{ij}^{k}(z_k^3 - z_{k-1}^3) \tag{3}$$

110 where $\bar{Q}_{ij}$ is the reduced stiffness of each ply, z is the position of the ply from the midplane and n is

111 the total plies in the laminate.

112 Then compound ABD matrix is inverted, which allows for the midplane strains, $\boldsymbol{\varepsilon}^0$, and curvatures,

113 K, to be determined for a given load using $\begin{Bmatrix} \boldsymbol{\varepsilon}^0 \\ K \end{Bmatrix} = \begin{bmatrix} A & B \\ B & D \end{bmatrix}^{-1} \begin{Bmatrix} N \\ M \end{Bmatrix}.$

114 By applying the measured normal compressive load, $N_{11} < 0$, the midplane strains for each

115 experiment can be obtained. Then, the stress state of a longitudinal ply can be determined with:

116 $$\boldsymbol{\sigma}_{long} = \bar{\mathbf{Q}}_{long}\boldsymbol{\varepsilon}^0 \tag{4}$$

117 Finally, if the material orientation of the ply does not coincide with the global coordinate system, as

118 is the case of the off-axis compression tests in section 3.3, this stress state is then rotated by the off-

119 axis angle, α, to give the local stresses in the material direction, $\boldsymbol{\sigma}^{\alpha} = \{\sigma_{11}\ \sigma_{22}\ \tau_{12}\}^T.$

120 $$\boldsymbol{\sigma}^{\alpha} = \mathbf{R}[\alpha]\boldsymbol{\sigma}_{long} \qquad \text{with} \quad \mathbf{R}[\alpha] = \begin{bmatrix} \cos[\alpha] & \sin[\alpha] & 0 \\ -\sin[\alpha] & \cos[\alpha] & 0 \\ 0 & 0 & 1 \end{bmatrix} \tag{5}$$


(a)   (b)

121
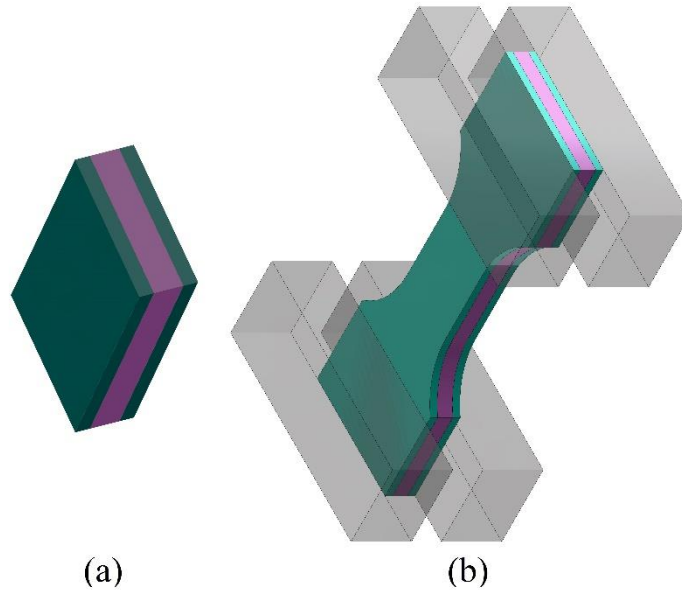
Figure 2. *Cross-ply laminate specimen designs: (a) rectangular (CP Cub), (b) clamped dog-bone (CP DBC).*

Finally, a series of off-axis CP specimens were cut at orientations of 3, 6, 10 and 15°. These tests were used to study the effects of combined in-plane shear and longitudinal compression on the fibre strength and evaluate available fibre kinking failure theories. Similar to the standard ±45° tension tests used to characterise the in-plane shear behaviour of composite laminates [13], the global response of the laminate can be considered as a superposition of its constituent plies following CLT only while there is no significant damage. The latter can cause considerable fibre rotation as well as inter and intra-laminar softening, making it difficult to decouple the behaviour of individual plies from the whole. Therefore, with these off-axis tests, a range of validity for the use of CP specimens in combined longitudinal compression and shear was determined. If the validity of this approach can be confirmed, the testing of compressive failure under combined loading would be greatly simplified in comparison to the ±5, ±10° laminates and tube specimens used in the past [14,15].

2.2 Experimental setup and data process

All the above experiments were conducted using a Zwick Roel 250 kN universal screw-driven testing machine under displacement control at a quasi-static loading rate of 0.01 mm/s. To ensure the alignment of the loading plates and avoid any eccentricity, the load was applied through two bearing balls an aligning frame, Figure 3, was installed. In addition, some cases required additional clamping fixtures, which are also shown in Figure 3.

7
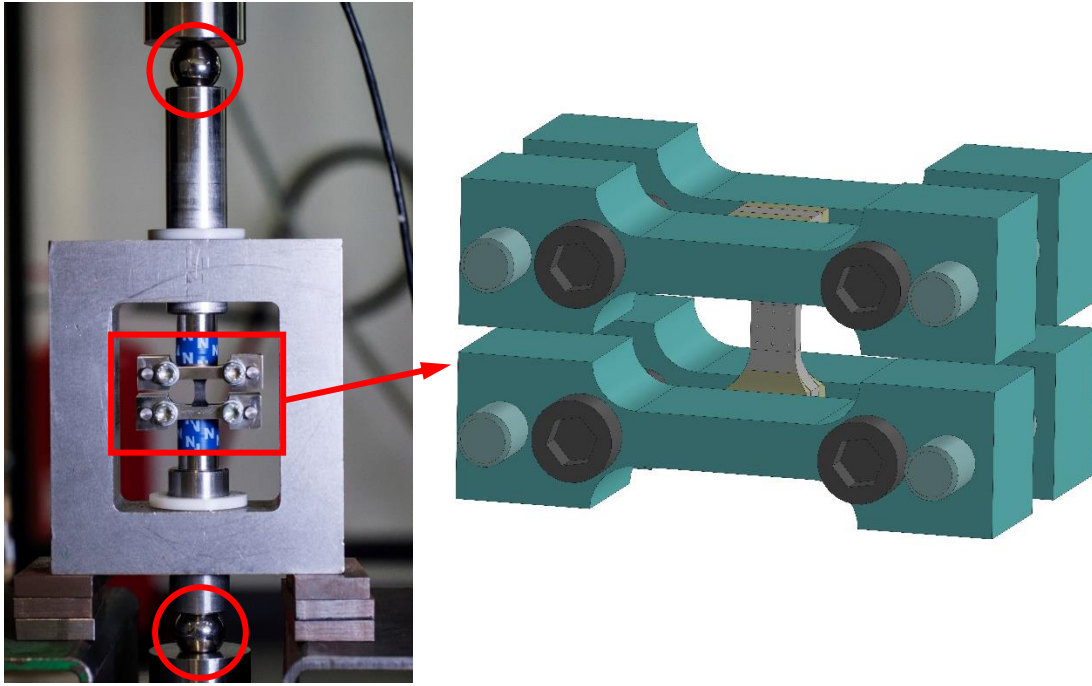
(a) Alignment fixture   (b) Specimen clamping fixtures

141   Figure 3. *Alignment and clamping fixtures used in fibre compression tests. (a) bearing balls (circled)*

142   *and alignment frame set-up, which ensures a strictly axial load is applied to the specimens, (b) close-*

143   *up view of the compact clamping fixtures is shown.*

144   Throughout the duration of the tests, force-displacement data was extracted at a 400 KHz sampling

145   rate from the test rig. In order to capture the deformation of the specimens throughout the tests with

146   Digital Image Correlation (DIC) techniques, a digital camera was set to record one picture of

147   approximately 70x120mm at a 512x760px resolution every second. These images, along with finely

148   sprayed black and white speckle patterns on the surface of the specimens, allowed for the calculation

149   of full field strain histories, obtained by post-processing with the DIC analysis software GOM

150   Aramis.

151   Finally, in the case of CP specimens, as long as the assumptions of small strains and linear behaviour

152   were fulfilled, longitudinal compression strengths were extracted from the global laminate response

153   using CLT following the method described in section 2.1 [11].

154   In addition, following the experiments, a number of samples were selected for closer post-failure

155   analysis using optical microscopy (OM) and scanning electron microscopy (SEM).

# 3   Experimental results

157   For each of the three sets of experiments described in the previous section, stress-strain curves and

158   specimen strengths were extracted and are discussed below. The baseline strength measurements

159   from the UD test results are reviewed and discussed in section 3.1. Next, the comparison of the CP

160   results against the baseline UD measurements is shown to establish the equivalence between the two

161   in section 3.2. Finally, in section 3.3, the off-axis CP test results are analysed to determine a range of

162   validity of the CLT method for the determination of UD compression strength and the effects of

163   shear on this mode of failure are investigated.

3.1   Unidirectional specimens

165   Four different types of UD specimens were tested to study the effects of the boundary conditions and

166   obtain the most accurate strength measurement for this particular IM7-8552 material system and give

167   reference strength values for the rest of the study. These results are summarised in Figure 4 and

168   Figure 5, which show the evolution of stress vs strain and a comparison of ultimate axial strengths

169   between the different specimen designs, respectively. Since all specimens had the same stiffness, for

170   the sake of clarity, only the rectangular and clamped dog-bone (DBC) specimens, which showed the

171   minimum and maximum strength values, are shown in Figure 4. For the full comparison, the reader

172   is referred to

173   *Figure* 5 and Table 1 where all the ultimate strength results of all four types of specimens can be

174   found. Unfortunately, due to the shape of the fixtures and clamps, only the front, or in-plane surface

175   was visible for all specimens so that there was no way to monitor out of plane bending in the tests.

176   This may have been the cause for the significant scatter observed for some of the specimen designs

177 and should be recorded, when possible. However, it should be noted that the selected cross-ply

178 designs showed good repeatability, as discussed in section 3.3.
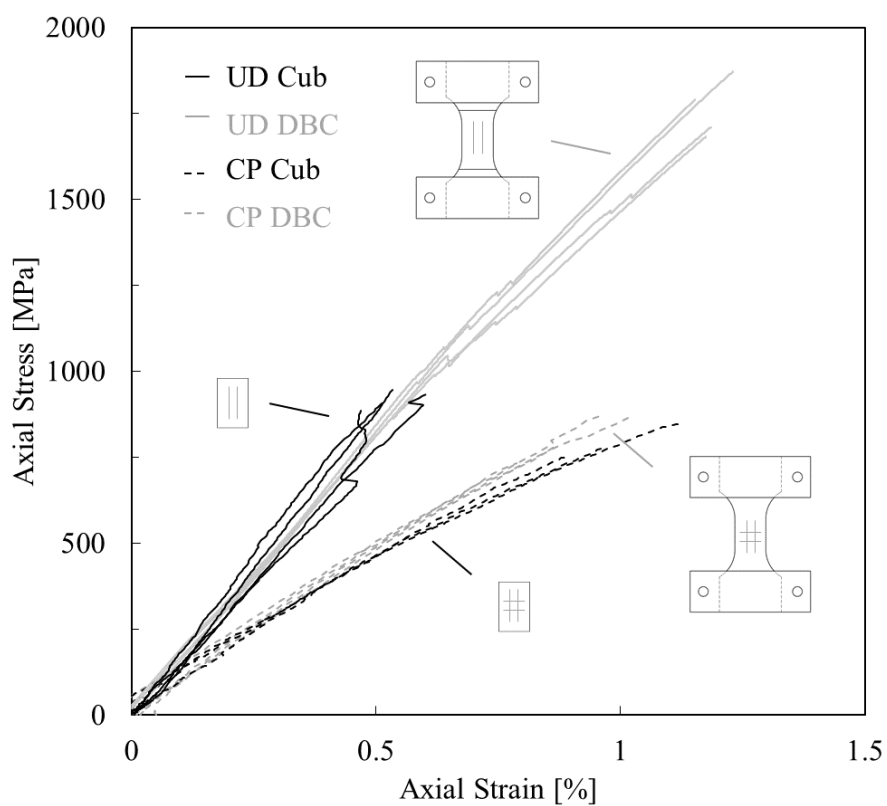
180 Figure 4. *Comparison between UD (DBC, Cub) and CP specimens (DBC, Cub) axial stress-strain*

181 *curves.*
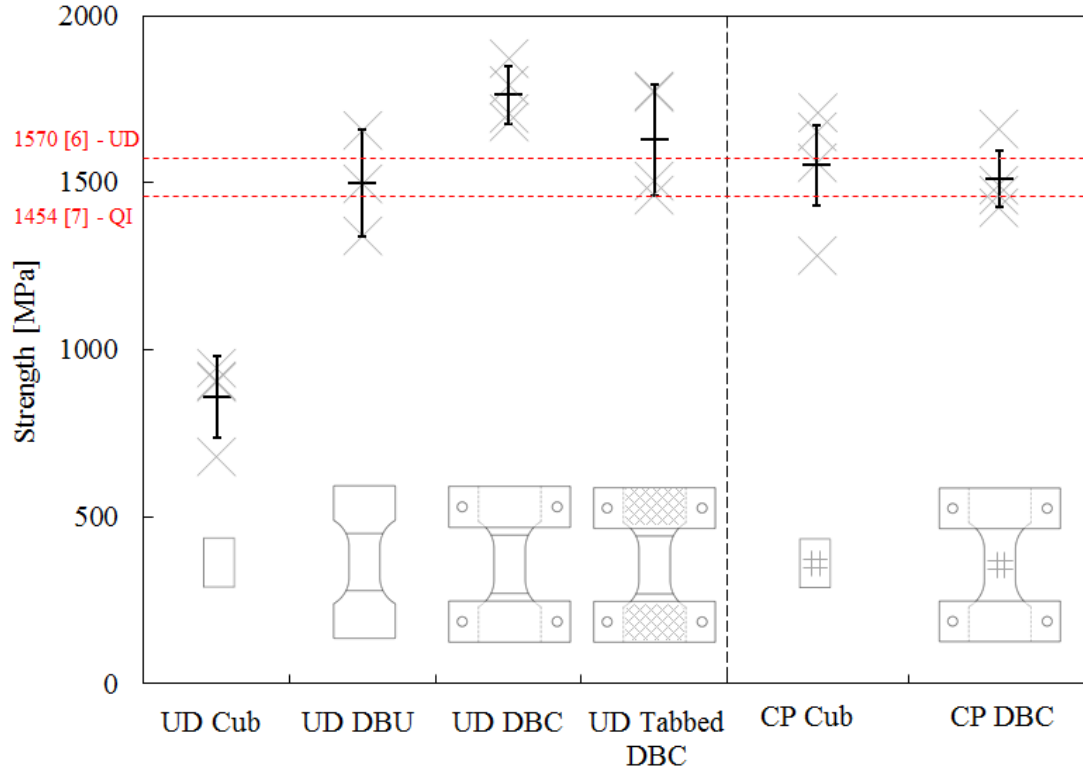
182

183   Figure 5. *Axial strength comparison between the four tested UD specimen designs (Cub, DBU, DBC*

184   *and Tabbed DBC) and two CP specimen designs (Cub and DBC) with literature data from IM7-8552*

185   *UD and QI specimens [6,7] added for reference. Black cross-marks in the figure represent the mean*

186   *and standard deviation for each specimen type.*

187   Table 1. *Summary of UD (Cub, DBU, DBC and Tabbed DBC) and CP (Cub, DBC) 0° compression*

188   *test results. The asterisk marks a specimen that may have failed early due to stress concentrations at*

189   *the boundary.*

Axial Strength	UD Cub [MPa]	UD DBU [MPa]	UD DBC [MPa]	UD Tabbed DBC [MPa]	CP Cub [MPa]	CP DBC [MPa]
1	679	1499	1873	1773	1283*	1661
2	903	1340	1790	1506	1651	1423
3	945	1659	1710	1772	1558	1463
4	907		1683	1462	1710	1494
5				1381		
AVG	859	1499	1764	1579	1551	1510

11

|						
STDV	121.2	159.5	85.6	182.6	189.2	104.6
CV (%)	14.1	10.6	4.9	11.6	12.8	6.9

190

191 As expected, the unclamped rectangular samples failed far below the expected fibre kinking strength

192 (1570 MPa) [6], at around 858 MPa on average. The specimens failed catastrophically due to matrix

193 splitting that originated at the loading boundaries before fibre failure could occur (see Figure 6 (a)).

194 The unclamped dog-bone specimens (DBU), which tried to mitigate the effect of stress

195 concentrations at the loading edges, showed a considerable increase in strength, reaching 1499 MPa

196 on average, but still ultimately failed due to matrix splitting, as can be seen in Figure 6 (b).

(a) Cub   (b) DBU
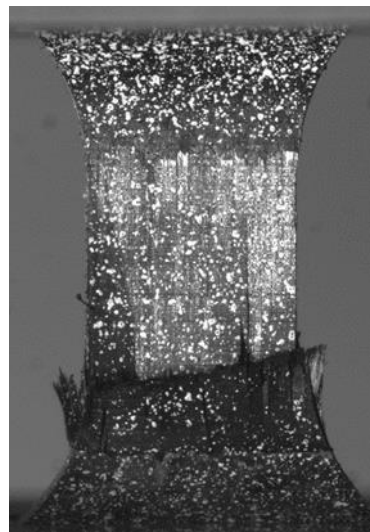
(c) DBC   (c) Tabbed DBC

Figure 6. *Failed UD specimens showing different observed failure modes: (a) Cub, (b) DBU, (c)*
DBC and (d) Tabbed DBC.

Therefore, it was necessary to resort to clamping fixtures, as used in [6–8], to apply combined loading compression (CLC, as described in ASTM D6641/D6641M) through combined end- and shear-loading at the clamps and strengthen the matrix in the transverse direction. However, the cited studies both reported kinking failure originating at the fixtures, likely caused by stress concentrations from the abrupt change in boundary conditions. The clamping fixtures were, therefore, used in combination with the dog-bone shaped specimens to reduce the effect of stress concentrations. Two different types of clamped specimen were tested, the simple dog-bone specimens (UD DBC), and the tabbed DBC specimens that included a layer of GFRP adhesively bonded to the composite below the clamped surface.

Even in the DBC specimens, some matrix cracking, as occurred in the DBU specimens, could not be completely prevented. However, in this case it only resulted in minor dips on the stress-strain curve, highlighted on the DBC curves in Figure 4, and did not significantly affect the stiffness, indicating that the load carrying ability was not affected. The DBC specimens continued to carry compressive loads far beyond this intermediate matrix splitting and eventually failed as desired in the form of kink bands within the gauge section, shown in Figure 6 (c), with an average strength of 1764 MPa.

On the other hand, the tabbed DBC specimen design was included to try and prevent the matrix splitting observed at the dog-bone radius in some of the DBC specimens. In addition, the direct

216 application of compressive fixtures could over-constrain the material and affect the fibre kinking

217 strength, dominated by localised matrix damage, which itself is strongly pressure-dependent [16–18].

218 Therefore, by relaxing the constraint on the UD material with the intermediate layer of GFRP

219 between the fixtures, some insight could be gained into the effects of boundary conditions on this

220 type of failure.

221 The tabbed DBC specimens failed at a much lower 1579 MPa on average but, interestingly, the

222 results appeared to fall into two groups based on their failure stress and observed damage mode,

223 although further testing would be required to verify this. One group of specimens failed below 1500

224 MPa with most specimens failing by matrix splitting as in the unclamped specimens and a couple of

225 cases of fibre kinking that initiated nearer to the boundary, possibly due to stress concentrations. The

226 second group failed at stress above 1700MPa, by kinking within the gauge section with no noticeable

227 matrix cracking (see Figure 6 (d)) and reached strengths very similar to the previous DBC specimen

228 design.

229 From these results, it appears that there are possibly two different failure modes under longitudinal

230 compression. For this specific IM7-8552 composite system, the combination of material properties

231 and fibre waviness are enough to cause matrix failure resulting in splitting and fraying at an axial

232 stress of around 1500 MPa, as observed in the unclamped DBU specimens and the first subgroup of

233 tabbed DBC specimens. However, the formation of kink bands did not occur until axial stress levels

234 between 1700-1800 MPa. It would seem that, for this fibre micro-buckling to occur, the material may

235 have to be over constrained to some degree, preventing matrix damage from resulting in splitting or

236 fraying, allowing the fibres to reach the higher buckling load.

237 **3.2   Cross-ply specimens**

238 In light of these issues with testing the thick UD specimens, a set of [0°/90°]$_{4S}$ cross-ply specimens

239 were tested following suggestions in the literature that multi-directional laminates may be better

240 suited for the determination of fibre kinking strength [6,7,11,19] as the transverse plies help to

241 reinforce the longitudinal fibres, allowing them to reach their buckling strength without the need for

242 additional external constraints.

243 For the cross-ply material, only two specimen designs were tested, an unclamped rectangular

244 specimen (CP Cub) and a clamped dog-bone specimen (CP DBC), shown in Figure 2. The results are

245 summarised in Table 1 and the axial stress-strain curves for both specimen types are shown in Figure

246 4 and

247 Figure 5. These also show the geometries and the extracted longitudinal compression strength next to

248 the UD specimen results. Since the stress-strain curves in Figure 4 showed no noticeable nonlinearity

249 and there were no signs of damage or fibre rotation in the specimens before fracture was observed,

250 the use of linear CLT for the extraction of longitudinal ply properties [11] was considered valid and

251 the ply strength data given in Table 1 and

252 Figure 5 is used for the rest of the discussion below.

253 As expected, both (CP Cub and CP DBC) geometries presented similar axial stiffness and practically

254 the same axial strength, with the Cub specimen showing slightly greater scatter. In addition, both

255 specimens failed within the gauge section, see Figure 7, due to fibre kinking originating in the central

256 plies and propagating outwards. Unfortunately, because of this, no particularly useful failure images

257 were captured on the outer layers during the test. However, section 4 includes more detailed

258 microscopy images of different off-axis specimens showing typical failure propagation through

259 longitudinal and transversal plies in CP specimens.

(a) Cub   (b) DBC
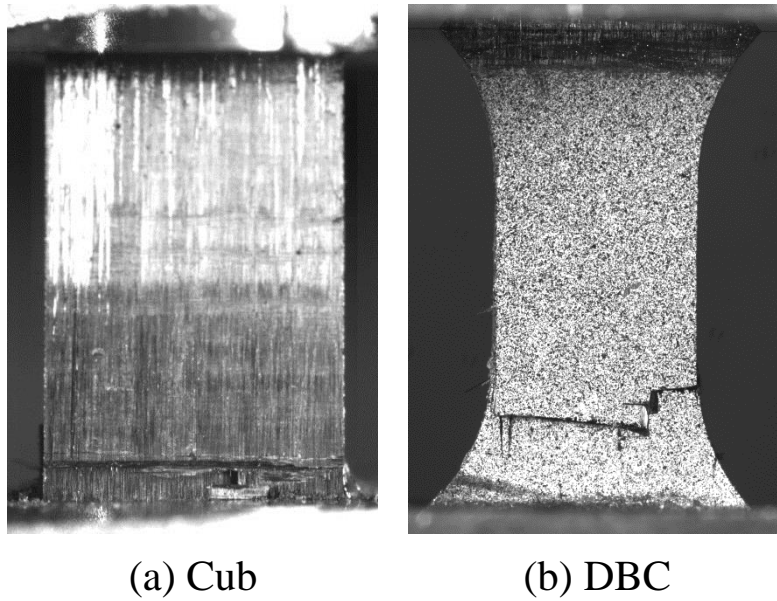
Figure 7. *Failed CP specimens showing failure on the outer plies after initiating and propagating outwards through the laminate. Left to right: (a) CP Cub and (b) CP DBC specimens.*

At a first glance, these results show that the practical issues encountered in testing the UD material are in fact avoided when testing the CP laminates, as no complex specimen design or fixtures are required to produce the desired mode of failure. In addition, the clamping fixtures did not appear to affect the compressive strength, although they may have improved experimental scatter. As a side note, however, significant experimental scatter is typically expected in this type of experiment due to the nature of the failure mode, which is caused by local fibre misalignments that can vary from one specimen to another. For reference, both the UD tests and the data from clamped QI specimens in [6,7] showed a similar variation in strength measurements.

However, when compared to the UD results from section 3.1, there are noticeable differences. Both CP specimens (CP Cub at 1551 MPa and CP DBC at 1510 MPa) failed at similar equivalent longitudinal ply strengths to the unclamped DBU and the subset of tabbed DBC specimens that failed due to matrix splitting. The UD specimens that reached fibre kinking strength, on the other hand, failed at around 1700 to 1800 MPa.

16

Previous studies on the same material showed longitudinal strength in QI laminates similar to that obtained here in the CP material and UD strength 10-20% lower [6,7]. However, UD specimens in both were reported to fail at the clamp edges, indicating that they may have suffered from critical stress concentrations, causing local matrix damage and premature onset of fibre kinking failure.

As discussed in the previous section, for the UD material it can be assumed that the material properties and local fibre misalignment (typically up to 3° [20]) result in the onset of Inter Fibre Failure (IFF) damage at longitudinal compressive loads of around 1500 MPa and the fibre micro-buckling strength, between 1700 and 1800 MPa, is only reached with sufficient additional constraints on the longitudinal fibres to make up for the reduced matrix support.

If similar material properties and fibre waviness to the UD laminate are assumed, it would seem that multi-directional laminates tend to fail at the onset of matrix damage, similar to the unconstrained UD specimens, whereas the stronger constraints on clamped UD specimens allows further matrix damage evolution and greater compressive loads before the constrained fibre buckling strength is reached.

Therefore, CP or other multi-directional laminates can be used to measure the longitudinal compression strength more reliably than UD material and without the need for complicated fixtures. In addition, if the objective is to characterise the behaviour of UD plies in a multidirectional laminate, taking into consideration possible size effects and differences in local fibre architecture such as those noted by Lee and Soutis [6], it may be argued that CP specimens will give a more representative measurement of the expected compressive strength. In fact, unidirectional material should be used with extreme caution as the material strength can very easily be under- or overestimated. Without the use of clamping fixtures, stress concentrations and edge effects can prematurely initiate matrix cracking and even fibre kinking as observed in the unclamped specimens in section 3.1 and in [6,7]. At the same time, the clamping fixtures can over constrain the material

299 and delay the onset of fibre buckling, resulting in greater observed ultimate strength than would be

300 possible otherwise.

3.3   Off-axis compression specimens

302 Having established the use of CP specimens for the measurement of the UD ply longitudinal

303 compression strength, a set of off-axis compression tests were carried out to determine range of

304 validity in combined loading, which is critical for the evaluation of 3D failure kinking theories. A

305 series of CP Cub samples cut at 0, 3, 6, 10 and 15° with respect to surface fibre direction were tested

306 in the same manner as the uniaxial compression test in section 3.2.

307 While the same was attempted for UD DBC and CP DBC specimen designs, these presented several

308 issues that made the data unreliable. In both cases, the waisted design of the specimens in

309 combination with the slight misalignment of the fibres, resulted in a non-uniform strain distribution

310 through the gauge section and stress concentrations at the change in section were greatly exaggerated

311 in the off-axis specimens, see Figure 8 (b). Because of this, it was difficult to accurately determine

312 the stress state at the point of failure and, therefore, directly extract a material property from the axial

313 measurements. In addition, in UD specimens, the same off-axis angles resulted in much greater shear

314 stresses, producing significant fibre rotation and changes in the failure mode from fibre buckling to

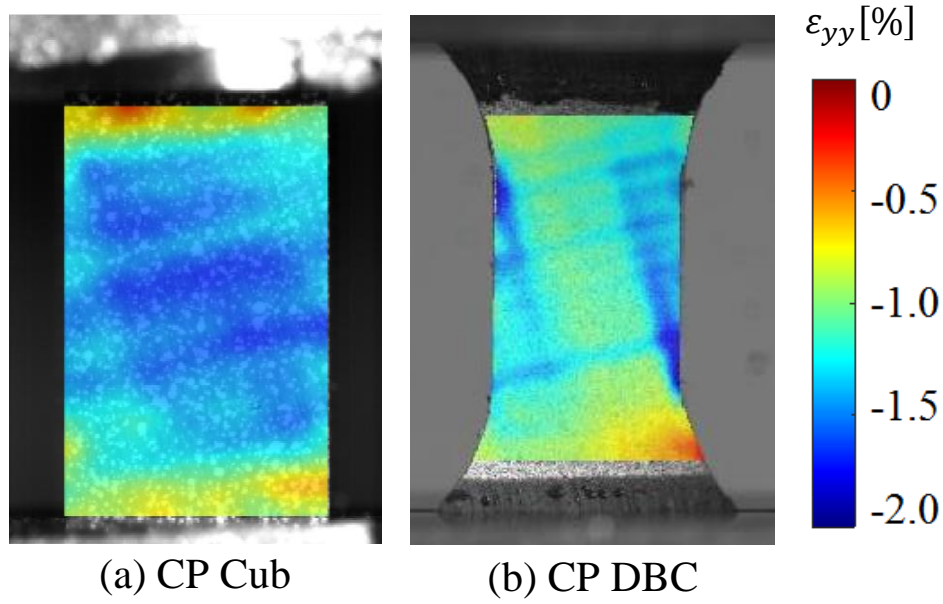315 matrix dominated shear banding.

(a) CP Cub   (b) CP DBC

316   Figure 8. *DIC longitudinal strain (ε_{yy}) overlay on two specimens showing non-uniform distribution in*

317   *a 15° off-axis CP DBC (b) compared to a 15° Cub specimen (a).*

318   In contrast, the rectangular CP specimens (see Figure 8 (a)) showed a much more uniform strain

319   distribution throughout the gauge section, which allowed for average axial stresses to be used more

320   reliably to extract individual ply stress states and ultimate strength measurements. Therefore, only

321   these were used in the off-axis compression study.

322   The axial data obtained for the off-axis CP Cub specimens is summarized in Table 2 and Figure 9,

323   which give the axial strength data and stress strain curves, respectively. A decrease in strength can be

324   observed as the off-axis angle increases, with noticeable nonlinearity in all specimens beyond 6°,

325   which also showed significant fibre rotation as the experiments progressed.

326   Table 2. *Summary of off-axis (0, 3, 6, 10 and 15°) CP Cub axial strength results.*

Axial Strength	CP Cub 0° [MPa]	CP Cub 3° [MPa]	CP Cub 6° [MPa]	CP Cub 10° [MPa]	CP Cub 15° [MPa]
1	747	744	623	467	341
2	783	746	643	468	353
3	847	741	706	452	353
4			630	451	350

19

|					
5				466	363
AVG	792	744	651	461	352
STDV	50.6	2.1	37.9	8.5	7.9
CV (%)	6.4	0.3	5.8	1.9	2.3

327

328
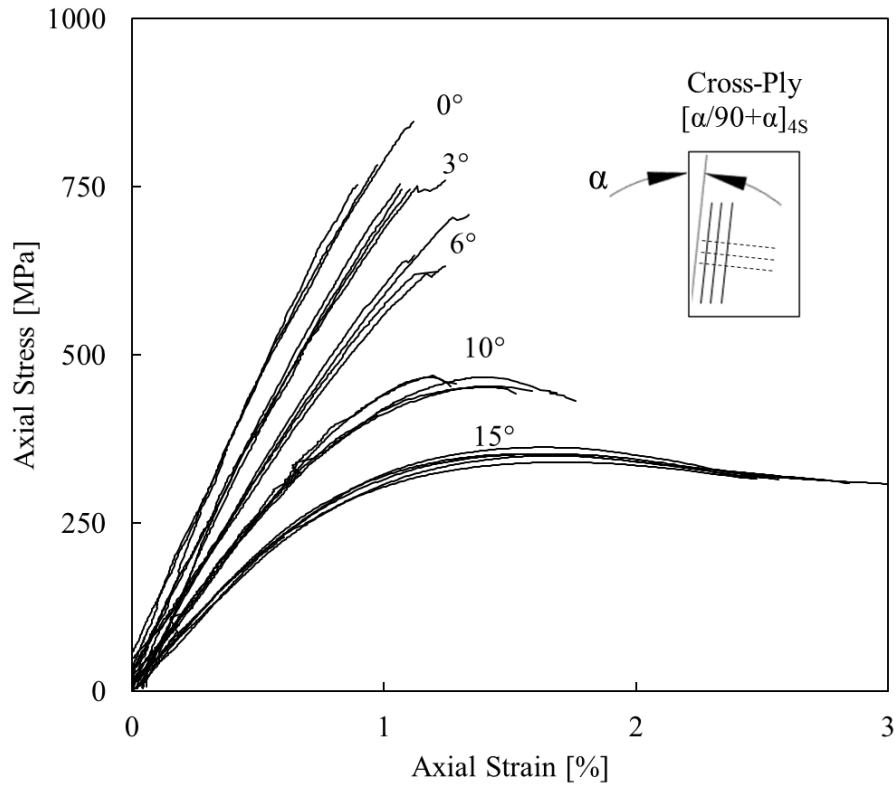
Figure 9. *Comparison of axial stress-strain curves for CP specimens with misalignment angles of 0,*
*3, 6, 10 and 15°.*

For a more in-depth look, macroscopic and SEM images in Figure 10 show the observed signs of fibre kinking failure in longitudinal plies and help to illustrate the differences in modes of failure between 3° , 6° and 10° specimens. For the lower off-axis specimens, from 0 to 6°, failure appeared to originate in the central longitudinal plies and propagate outwards, with the fibres tending to buckle in the out-of-plane direction. Conversely, for the 10 and 15° specimens, ultimate failure was preceded by significant shear non-linearity, which seemed to promote buckling in the same direction, keeping it more contained within the plane.
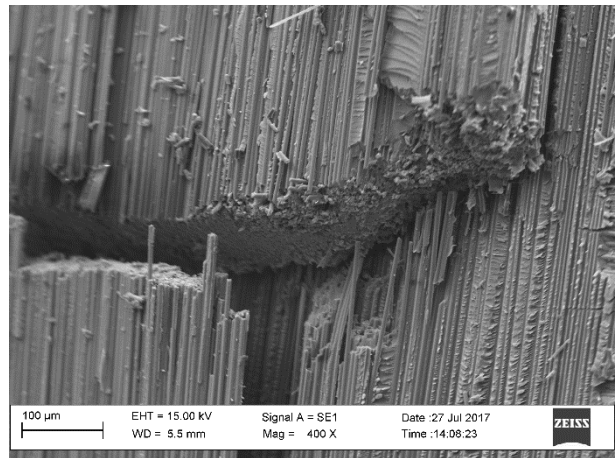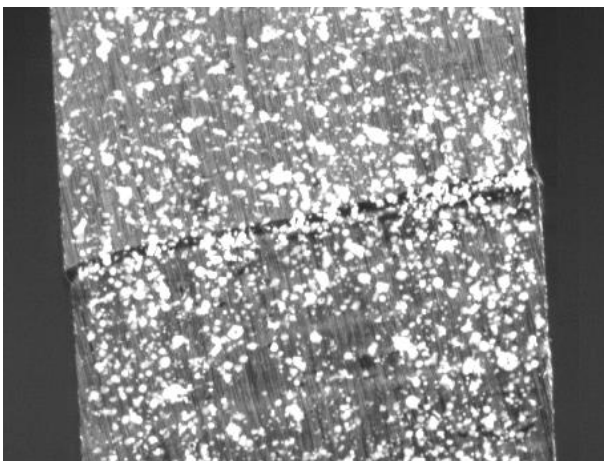
(a) 3° CP - failure surface
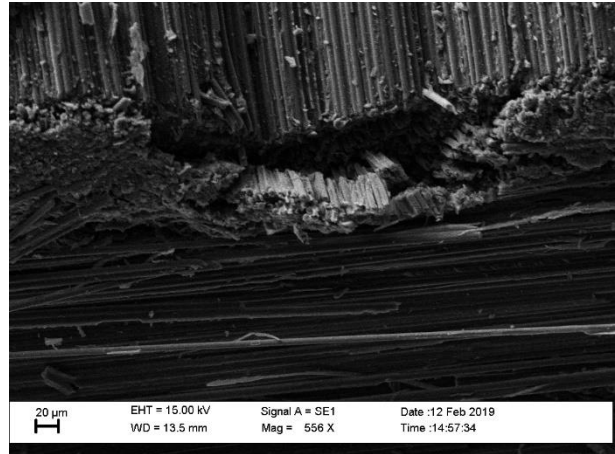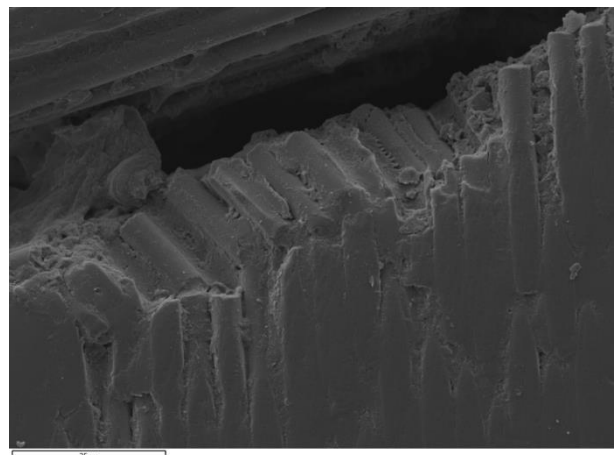
(b) 3° CP - through thickness SEM
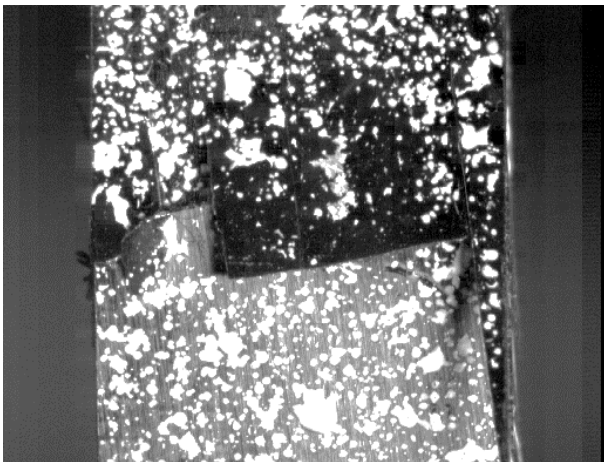
(c) 6° CP - failure surface

(d) 6° CP - through thickness SEM

(e) 10° CP - failure surface

(f) 10° CP - through thickness SEM

338   Figure 10. *Macroscopic (digital camera) and Scanning Electron Microscope (SEM) images of*

339   *different failed 3, 6 and 10° CP specimens showing signs of fibre kinking failure. Scale bars indicate*

340   *20 μm in (b), 100 μm in (d), and 25 μm in (f).*

341   Up to 6°, however, there was no noticeable nonlinearity and no signs of damage or fibre rotation in

342   the specimens before the point of failure. In addition, shear stress–strain curves for the same IM7-

343   8552 material in [21,22] show significant nonlinearity starting only after shear stresses of around 60-

344   70 MPa and both the 3 and 6° tests fall below that limit (see Figure 11). Therefore, for these

345   specimens, an accurate estimate of the internal stress state in the longitudinal plies can be obtained

346   using linear CLT, as was done for the uniaxial compression tests in section 3.2, and the use of CP
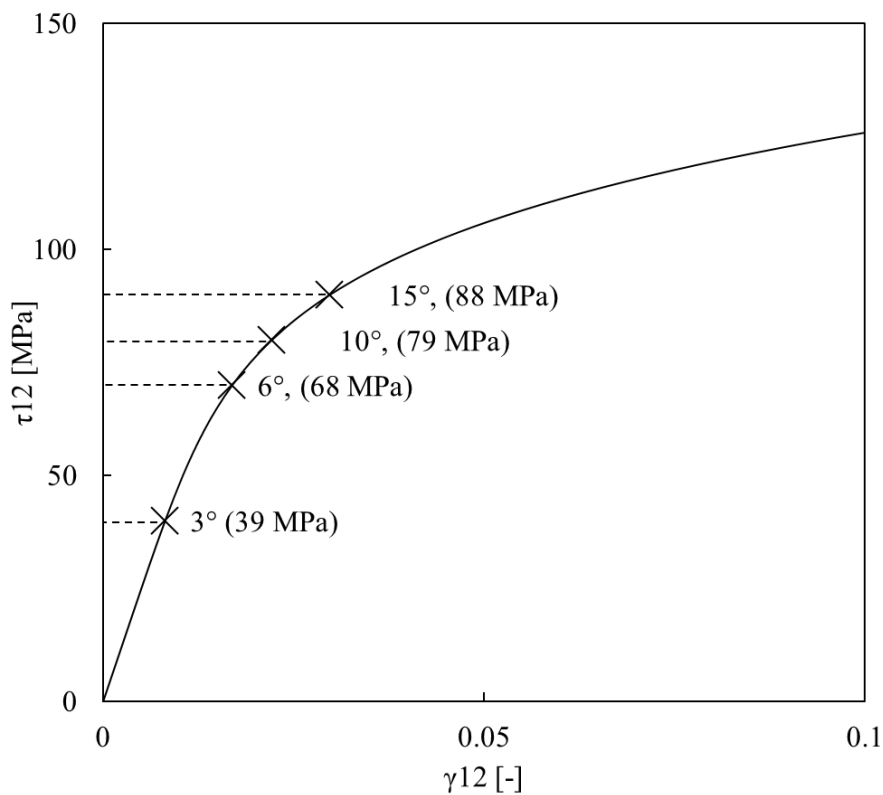
347   material instead of UD can be considered valid.

348

349   Figure 11. *Average shear stresses from the 3 and 6° off-axis compression tests overlaid on the*

350   *experimental shear stress–strain curve for an IM7-8552 composite, reproduced from* [22].

351   4   Discussion and analysis

352   Based on all the results gathered above, simple CP specimens can be used to determine the

353   longitudinal compression strength of unidirectional composite material in both uniaxial and off-axis

354 compression tests, without the need for complex fixtures, for as long as the stress-strain curves

355 remain linear. In this case, for the IM7-8552 composite, this limit was found at around 6° when the

356 shear stresses in the laminate reached around 60-70 MPa. For greater off-axis angles, useful data

357 cannot be simply extracted using linear CLT and a more rigorous analysis would be required, giving

358 consideration to the nonlinear behaviour of the material, possible interlaminar damage, and fibre or

359 specimen rotation.

360 For the uniaxial compression case, various different UD specimen designs were tested to obtain a

361 reliable reference measure of the material's compressive strength. From these tests a serious

362 difficulty in reaching the desired fibre micro-buckling failure mode was noted. Firstly, waisted, or

363 dog-bone, specimen designs were necessary to avoid stress concentrations at the edges causing

364 premature failure.

365 However, even then, there appear to be two different mechanisms dictating the compressive strength

366 of the material depending on the boundary conditions of the experiment. For tests with more relaxed

367 lateral constraints, including completely unclamped and clamped specimens with GFRP end tabs

368 between the clamping fixtures, the material tended to fail due to matrix cracking and fibre kinking

369 was rarely produced. On the other hand, fibre kinking, or micro-buckling, failure was only

370 consistently achieved when the specimens were over-constrained, with the clamping fixtures

371 possibly maintaining alignment of the fibres beyond the IFF failure of the matrix. Between these two

372 different scenarios, matrix failure measured at around 1500 MPa, while the over-constrained fibre

373 kinking mode was measured at over 1700 to 1800 MPa.

374 From this it was concluded that: (i) reliable compression strength measurements were extremely

375 difficult to achieve with UD material; and (ii) the compressive failure of the laminate was caused by

376 failure of the supporting matrix, at around 1500 MPa.

377   In second place, two different CP specimen designs were tested to compare against the UD results, a

378   rectangular unclamped specimen and a clamped dog-bone design. The two different specimens

379   showed no significant differences between them, regardless of shape or the use of clamping fixtures,

380   indicating reliable material and test design. Not only that, but the extracted longitudinal compression

381   strength using CLT [11] coincided with the measured UD results at 1500 MPa. Therefore, CP

382   laminates have been shown to produce accurate results for longitudinal compressive strength and,

383   due to greater reliability and lower sensitivity to boundary conditions, it is strongly recommended to

384   use this type of material over UD laminates. In addition, fibre kinking strength is dependent on local

385   fibre architecture and, therefore, a cross-ply, or quasi-isotropic, layup will better characterize the

386   behaviour of multi-directional laminates, which are more typically used in engineering applications.

387   Finally, for the case of off-axis compression, the same CP material was used to prepare angled

388   specimens cut at 0, 3, 6, 10 and 15° from the fibre direction. These showed that, as long as the

389   resultant stress-strain curves remained linear, the assumptions of CLT remained valid and the effects

390   of combined loading on the compressive strength could be measured the same specimen/test design

391   as the previous uniaxial compression tests.

392   Shuart et al. in 1989 and Soden et al. in 2002 used ±5 and ±10° angle-ply specimens and

393   unidirectional tubes, respectively, to study the longitudinal compressive strength of fibre composites

394   under combined loading [14,15]. The effects of shear on longitudinal compression strength observed

395   in the present study follow a similar trend to the results from [14,15], shown normalised against the

396   uniaxial compression strength for each material in Figure 12 for a clearer comparison, which adds

397   confidence in the validity of the proposed specimen design. In addition, the CP specimen presents

398   several advantages over previous approaches: the CP material is more readily available and multiple

399   different orientations can be obtained from a single laminate, making it a more versatile, cost-

400   effective and convenient method to test different shear–longitudinal compression ratios.
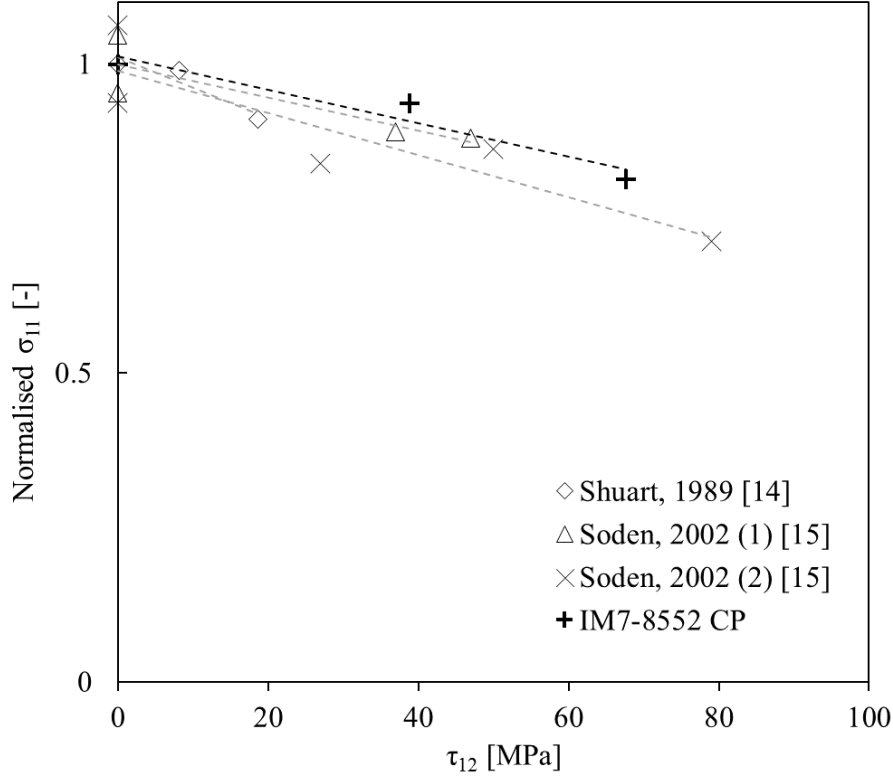
401

402 Figure 12. *Comparison of combined longitudinal compression and in-plane shear test results*

403 *between different materials and test methods in the literature* [14,15] *and the new results presented*

404 *in this article. Two different data sets from* [15] *are included. Results are shown normalised with the*

405 *uniaxial compression strength for each material.*

406 Finally, the obtained results were used to evaluate the fibre kinking theory proposed by Pinho in [5],

407 which is one of the few criteria for this type of failure with a sound physical explanation

408 implemented in three dimensions and has been shown to produce good results in the uniaxial

409 compression case [23]. This theory consists in rotating the macroscopic stress state to an internal

410 misalignment frame, Figure 13 (a), obtained by adding the local shear strain to the initial fibre

411 waviness.

412 $$\sigma^m = R[\varphi]\sigma^\psi \tag{6}$$

413 $$\varphi = \text{sign}[\tau_{12}^\psi]\varphi^0 + \gamma_m \tag{7}$$

25

414 Where φ is the misalignment angle, φ^0 is the initial misalignment, and γ_m is the shear strain in the

415 misalignment frame. The kink-band stress, $\boldsymbol{\sigma}^\psi = \mathbf{R}[\psi]\boldsymbol{\sigma}$, is obtained in a similar manner by rotating

416 the Cauchy stress vector, $\boldsymbol{\sigma}$, to the kink-band plane with the angle, ψ, found numerically.

417 The local misalignment frame stresses are then used to evaluate the fibre finking criterion, where

418 failure can occur by instability of the additional fibre rotation, if γ_m, which is solved iteratively, does

419 not have a stable solution, or by matrix fracture, if γ_m is stable and:

420 $$f_{\text{kink}} = f_{\text{IFF}}[\boldsymbol{\sigma}^m] = 1 \qquad (8)$$

421 Where the kinking criterion, f_{kink}, is evaluated as an IFF criterion of the type described in [4,5,24]

422 on the misalignment frame, $f_{\text{IFF}}[\boldsymbol{\sigma}^m]$. A more detailed explanation and subsequent simplifications

423 made over the years to avoid iteration can be found in [3–5], however only the original, numerically

424 intensive, implementation has been used here to prevent any possible loss of accuracy.

425 When used to study the present off-axis CP experiments, however, this theory, as originally

426 described in [25], appears to over predict the effect of shear. Predictions are shown next to

427 experimental results in terms of longitudinal (σ_{11}) vs shear (τ_{12}) stress at failure in Figure 14.

428 However, with a minor modification, predictions can be greatly improved for cases with combined

429 shear. The proposed modification consists in replacing the misalignment frame shear strain, γ_m, from

430 (7) with a relative shear strain measure, γ_m^r, shown below.

431 $$\gamma_m^r = f_{\text{CL}}[\tau_{12}^r] = f_{\text{CL}}\left[\tau_{12}^m - \tau_{12}^\psi\right] \qquad (9)$$

432 In an analogous way, γ_m^r is obtained from the very same constitutive law ($f_{CL}[\tau_{12}^r]$) employed

433 previously to calculate γ_m. However, now a relative shear stress, τ_{12}^r, is used instead of τ_{12}^m. In this

434 way, as the global fibre direction rotates with τ_{12}^ψ, only the shear strain relative to the current material

435 orientation is considered for the misalignment angle calculation. Otherwise, the local fibre rotation is

436   overestimated as illustrated in Figure 13 (b), where φ is the misalignment angle computed per

437   Pinho's original implementation, while φ^* is the angle corresponding to the proposed modification.

$$(\varphi = \varphi^0 + \gamma_m) \qquad (\varphi^* = \varphi^0 + \gamma_m^r)$$
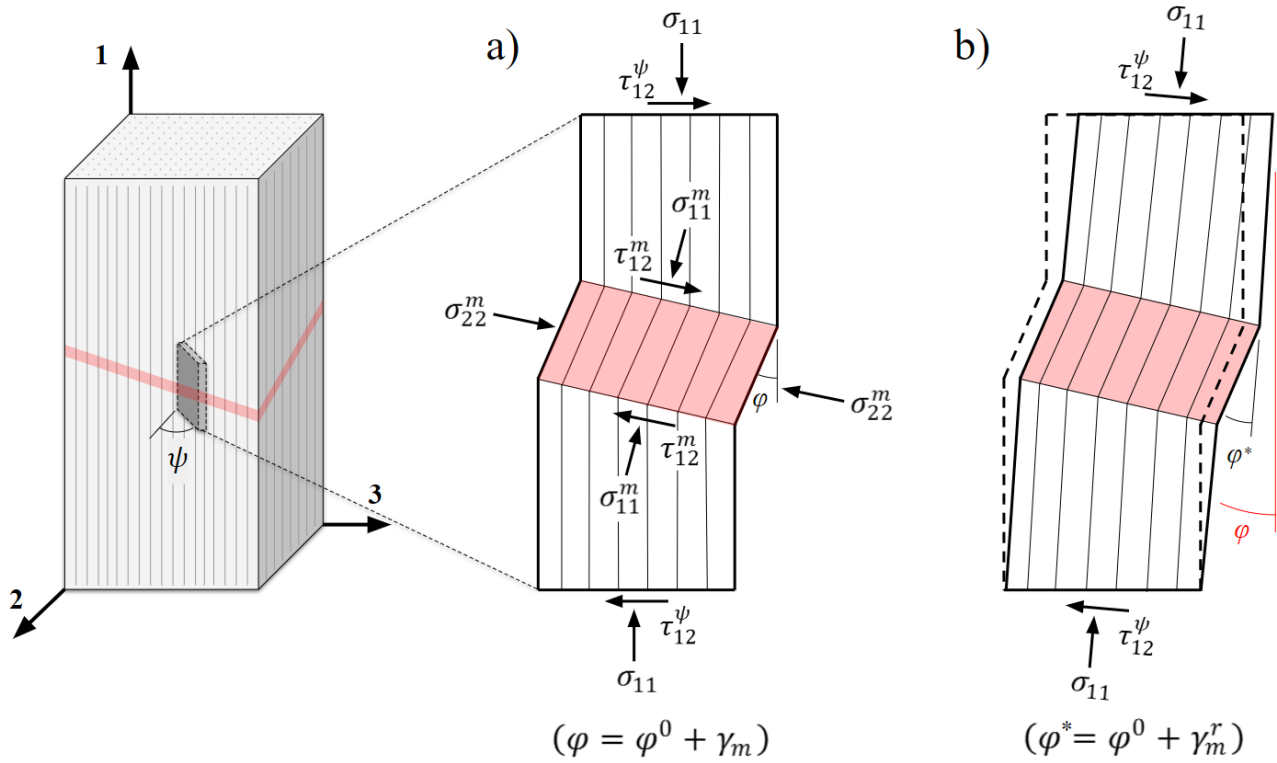
438

439   Figure 13. a) *Kink-band and misalignment planes according to fibre kinking theory* [1,2,5] *and b)*

440   *effect of considering the proposed relative shear vs the global shear for the misalignment angle, φ.*

441   Both models were calibrated with the average uniaxial compression strength and shear stress–strain

442   behaviour from [14,15] and gave an initial misalignment angle of 1.85°, which falls within typical

443   expected values and matches the analytical solution for the uniaxial compression case as described in

444   [26]. With the proposed modification, the solution remains unchanged for the pure compression case

445   but, for off-axis compression cases, there are some noticeable improvements. In the 0° and 3° tests,

446   the longitudinal compression strength (σ_{11}) remains constant as the local shear stress in the

447   misalignment frame remains in the linear elastic region and buckling occurs purely due to

448   mechanical instability of the misaligned fibres. Beyond this point, the greater shear stresses cause

449   matrix failure in the local misalignment frame before the instability condition is met, with

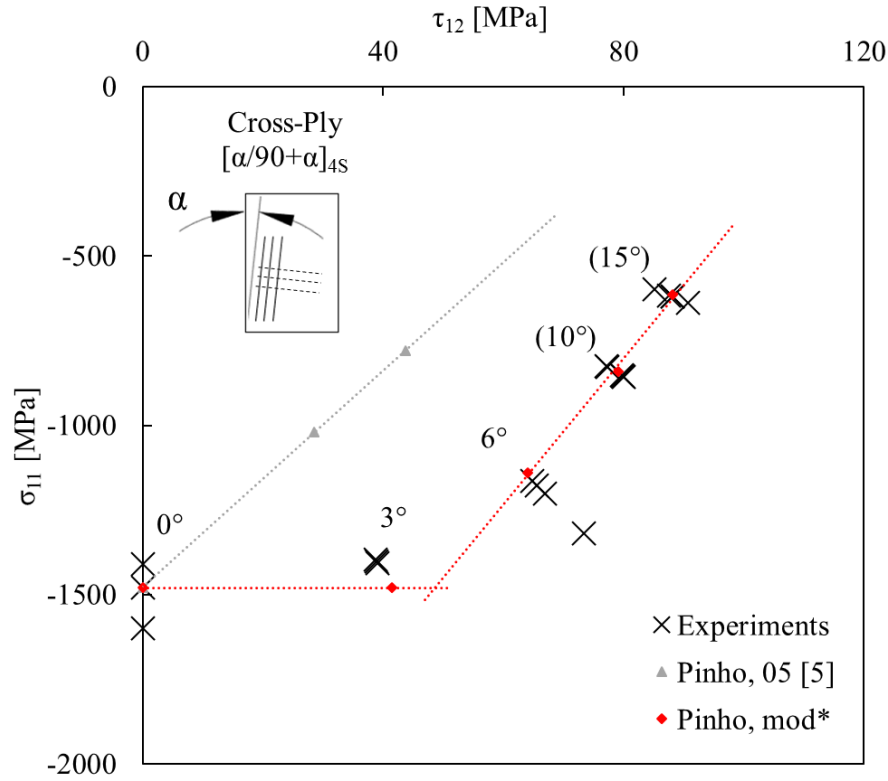450   subsequent micro-buckling occurring because of this.

451

Figure 14. *Longitudinal (σ_{11}) vs shear (τ_{12}) stress at failure for the 0, 3, 6, 10 and 15° CP Cub*

specimens, extracted using CLT. Brackets on 10 and 15° results indicate that a corrwecting factor

has been applied to correct for fibre rotation. Grey markers indicate predicted failure stresses for

each case using the fibre kinking theory proposed by Pinho [5] *and red markers indicate predictions*

using the proposed modification. Numerical predictions were only calculated for the five off-axis

loading cases, dotted trend lines are extrapolated from these results.

This change in predicted cause of failure, from mechanical instability to IFF failure of the supporting

matrix, seems to agree well with the experimental results, which show little effect of the shear stress

between the 0° and 3° tests followed by a significant drop as the off-axis angle increases. In addition,

it would also help to explain the differences observed in the experiments (Figure 10), as the failure

mode appears to become more stable and matrix dominated with greater off-axis angles.

Overall, however, these results show that there is still work to be done on the prediction of fibre

kinking failure under combined, or off-axis, loads. Complex physically-based criteria like Pinho's,

465 appear unable to capture the effects of shear, indicating that some of the driving failure mechanisms

466 may not yet be fully understood. The proposed modification to Pinho's criteria suggests one potential

467 explanation but may still be a pragmatic simplification of the micro-scale fibre rotation and matrix

468 damage mechanisms. Therefore, while the initial results appear to show good agreement, further

469 research is needed on the micro-mechanical behaviour of fibre composites under combined

470 compression and shear.

471 **5   Conclusions**

472 A series of longitudinal compression tests have been carried out on unidirectional and cross-ply

473 IM7/8552 composite laminates, with the aim of finding an optimal test method for the determination

474 of fibre compression strength.

475 For the UD samples, it resulted extremely challenging to produce reliable measurements, as the

476 material proved highly sensitive to specimen geometry and boundary conditions. The CP specimens,

477 on the other hand, produced much more reliable results, which were not noticeably affected by either

478 specimen geometry or boundary conditions.

479 Therefore, considering the fact that the CP samples are also better than UD ones in representing

480 practical multi-directional structures, the cubic CP sample is recommended throughout this work for

481 characterizing fibre kinking strength.

482 In addition, the same CP specimen design was used with fibre orientations of 0, 3, 6, 10 and 15

483 degrees to the loading axis to study the effect of shear on the fibre compression strength. This proved

484 to be a reliable and much simpler approach to obtaining this type of data compared to previous

485 experiments in the literature and provided additional data points for the evaluation of fibre

486 compression failure criteria.

487 Finally, this data was used to evaluate the fibre kinking theory proposed by Pinho in [5] and a minor

488 modification is proposed, which improves predictions in cases with combined longitudinal

489 compression (σ_{11}) and in-plane shear (τ_{12}).

References

494 [1] Rosen BW. Mechanics of composite strengthening. Fiber Compos. Mater. Semin. Am. Soc.

495   Met., Ohio: American Society for Metals; 1965, p. 37–75.

496 [2] Budiansky B, Fleck NA. Compressive failure of fibre composites. J Mech Phys Solids

497   1993;41:183–211. doi:10.1016/0022-5096(93)90068-Q.

498 [3] Pinho ST, Iannucci L, Robinson P. Physically-based failure models and criteria for laminated

499   fibre-reinforced composites . Part I: Development. Compos Part A Appl Sci Manuf

500   2006;37:63–73. doi:10.1016/j.compositesa.2005.04.016.

501 [4] Pinho S, Darvizeh R, Robinson P, Schuecker C, Camanho P. Material and structural response

502   of polymer-matrix fibre-reinforced composites n.d. doi:10.1177/0021998312454478.

503 [5] Pinho ST, Dávila CG, Camanho PP, Iannucci L, Robinson P. Failure Models and Criteria for

504   FRP Under In-Plane or Three-Dimensional Stress States Including Shear Non-linearity. Tm-

505   2005-213530 2005:68. doi:NASA/TM-2005-213530.

506 [6] Lee J, Soutis C. A study on the compressive strength of thick carbon fibre–epoxy laminates.

507   Compos Sci Technol 2007;67:2015–26. doi:10.1016/j.compscitech.2006.12.001.

508 [7] Ploeckl M, Kuhn P, Grosser J, Wolfahrt M, Koerber H. A dynamic test methodology for

509   analyzing the strain-rate effect on the longitudinal compressive behavior of fiber-reinforced

510   composites. Compos Struct 2017;180:429–38. doi:10.1016/j.compstruct.2017.08.048.

511   [8]   ASTM D6641 / D6641M - 09 Standard Test Method for Compressive Properties of Polymer

512   Matrix Composite Materials Using a Combined Loading Compression (CLC) Test Fixture

513   2009. doi:10.1520/D6641_D6641M-09.

514   [9]   Kaddour A, Hinton M, Smith P, Li S. Mechanical properties and details of composite

515   laminates for the test cases used in the third world-wide failure exercise. J Compos Mater

516   2013;47:2427–42. doi:10.1177/0021998313499477.

517   [10] Johnson W, Masters J, Wilson D, Welsh J, Adams D. Unidirectional Composite Compression

518   Strengths Obtained by Testing Cross-Ply Laminates. J Compos Technol Res 1996;18:241.

519   doi:10.1520/CTR10109J.

520   [11] Welsh JS, Adams DF. Testing of angle-ply laminates to obtain unidirectional composite

521   compression strengths. Compos Part A Appl Sci Manuf 1997;28:387–96. doi:10.1016/S1359-

522   835X(96)00138-8.

523   [12] Hexcel. HexPly 8552 Data Sheet. n.d.

524   [13] Lafarie-Frenot MC, Touchard F. Comparative in-plane shear behaviour of long-carbon-fibre

525   composites with thermoset or thermoplastic matrix. Compos Sci Technol 1994;52:417–25.

526   doi:10.1016/0266-3538(94)90176-7.

527   [14] Shuart MJ. Failure of compression-loaded multidirectional composite laminates. AIAA J

528   1989;27:1274–9. doi:10.2514/3.10255.

529   [15] Soden PD, Hinton MJ, Kaddour AS. Biaxial test results for strength and deformation of a

530   range of E-glass and carbon fibre reinforced composite laminates: failure exercise benchmark

531   data. Compos Sci Technol 2002;62:1489–514. doi:10.1016/S0266-3538(02)00093-3.

532   [16] Hine PJ, Duckett RA, Kaddour AS, Hinton MJ, Wells GM. The effect of hydrostatic pressure

533 on the mechanical properties of glass fibre/epoxy unidirectional composites. Compos Part A

534 Appl Sci Manuf 2005;36:279–89. doi:10.1016/j.compositesa.2004.06.004.

535 [17] Shin ES, Pae KD. Effects of Hydrostatic Pressure on In-Plane Shear Properties of

536 Graphite/Epoxy Composites n.d.

537 [18] Hoppel CPR, Bogetti TA, Gillespie JW. Literature Review-Effects of Hydrostatic Pressure on

538 the Mechanical Behavior of Composite Materials. J Thermoplast Compos Mater 1995.

539 doi:10.1177/089270579500800403.

540 [19] Welsh JS, Adams DF. An Experimental Investigation of the Mini-Sandwich Laminate as Used

541 to Obtain Unidirectional Composite Compression Strengths. J Compos Mater 1997;31:293–

542 314. doi:10.1177/002199839703100304.

543 [20] Czabaj MW, Riccio ML, Whitacre WW. Numerical reconstruction of graphite/epoxy

544 composite microstructure based on sub-micron resolution X-ray computed tomography.

545 Compos Sci Technol 2014;105:174–82. doi:10.1016/J.COMPSCITECH.2014.10.017.

546 [21] Erice B, Thomson D, Ponnusami SA, Pathan M V., Petrinic N. On the Rate-dependent

547 Plasticity Modelling of Unidirectional Fibre-reinforced Polymeric Matrix Composites. EPJ

548 Web Conf 2018;183:01055. doi:10.1051/epjconf/201818301055.

549 [22] Koerber H, Xavier J, Camanho PP. High strain rate characterisation of unidirectional carbon-

550 epoxy IM7-8552 in transverse compression and in-plane shear using digital image correlation.

551 Mech Mater 2010;42:1004–19. doi:10.1016/j.mechmat.2010.09.003.

552 [23] Naya F, Herráez M, Lopes CS, González C, Van der Veen S, Pons F. Computational

553 micromechanics of fiber kinking in unidirectional FRP under different environmental

554 conditions.   Compos   Sci   Technol   2017;144:26–35.

555 doi:10.1016/J.COMPSCITECH.2017.03.014.

556 [24] Puck A, Schürmann H. FAILURE ANALYSIS OF FRP LAMINATES BY MEANS OF

557   PHYSICALLY BASED PHENOMENOLOGICAL MODELS. Compos Sci Technol

558   1998;58:1045–67. doi:10.1016/S0266-3538(96)00140-6.

559 [25] Pinho ST. Modelling failure of laminated composites using physically-based failure models.

560   2005.

561 [26] Bergan A, Herráez M, González C, Lopes C. Development of a Mesoscale Finite Element

562   Constitutive Model for Fiber Kinking. 2018 AIAA/ASCE/AHS/ASC Struct. Struct. Dyn.

563   Mater. Conf., Reston, Virginia: American Institute of Aeronautics and Astronautics; 2018.

564   doi:10.2514/6.2018-1221.

565

A study on the longitudinal compression strength of fibre reinforced composites under uniaxial and off-axis loads using cross-ply laminate specimens.

Thomson, Daniel